Binary Fe-Pd submicron structures fabricated through glancing angle deposition (GLAD) for bioapplications

Uta Allenstein[a,b,1], Emilia I. Wisotzki[a,1], Christine Gräfe[c], Joachim H. Clement[c], Yanhui Liu[b], Jan Schroers[b], S. G. Mayr[a,*]

[a] *Leibniz-Institute for Surface Modification (IOM), Leipzig, Germany and Division of Surface Physics, Department of Physics and Earth Sciences, University of Leipzig, Germany*
[b] *Department of Mechanical Engineering and Materials Science, Yale University, New Haven, Connecticut 06511, USA*
[c] *Clinic of Internal Medicine II, Department of Haematology and Medical Oncology, Jena Universital Hospital, Jena, Germany*

Abstract

Fe_7Pd_3 structured thin films were synthesized using glancing angle deposition (GLAD), motivated by the high potential for use of such structures in magnetically-controlled bioapplications. Specifically, GLAD of Fe-Pd was carried out on prestructured gold templates to obtain Fe-Pd structures of several hundred nanometers in width by up to 1.5 µm in length, depending on the template and growth parameters. The resulting polycrystalline microstructure was in the body centred cubic (bcc) phase with a composition near Fe_7Pd_3, as determined by energy-dispersive X-ray spectroscopy (EDS) and X-ray diffraction (XRD). Annealing at 900 °C resulted in appearance of signatures of the face centered tetragonal (fct) martensitic phase within XRD measurements. Therefore, fct submicron colums could be achieved if appropriate measures for structural preservation are taken, such as by ultra rapid annealing or lift-off prior to annealing. The cellular response to the structured films was investigated using human brain microvascular endothelial cells (HBMEC) and revealed consistent cell adhesion, morphologies and proliferation in comparison to control Fe-Pd and Si substrates. Furthermore, only trace amounts of palladium and iron were released from the films into the growth medium during the culture time,

*Corresponding author
[1] Shared first authorship

regardless of the structures. Overall, this method is highly promising for the development of biocompatible, submicron structured films and shape-anisotropic ferromagnetic micro- and nanostructures, with applicability to a range of other alloys.

Keywords: Glancing angle deposition (GLAD), iron palladium alloy, Fe-Pd submicron structures, magnetically-responsive material, shape memory effect

1. Introduction

Fe-Pd alloys around the composition Fe_7Pd_3 constitute a highly versatile class of functional materials with significant potential in biomedical applications. Through appropriately tuning phase and structure, e.g. via careful choice of the stoichiometry and annealing treatment, these alloys have not only demonstrated the Invar effect over a broad temperature range [1], but also a pronounced magnetocrystalline anisotropy [2] and, most recently, the ferromagnetic shape memory effect [3]. While the former effect is primarily of interest for conventional engineering applications [4], the latter two pose enormous potential for biomedical applications including magnetically-driven actuators and sensors, given the low toxicity of Fe-Pd in comparison to other magnetic shape memory alloys [5].

Fe-Pd combines the ferromagnetic properties of iron with the highly biocompatible properties of the precious metal palladium [6], resulting in an alloy that is both resistant to corrosion and highly ductile [7, 2]. Pure Fe-Pd is established to act as a ferromagnetic shape memory alloy if residing in the face centred tetragonal (fct) martensitic phase [3, 8]. Such Fe-Pd thin films have been the focus of significant research, primarily for magnetically responsive shape memory devices (e.g. [9, 10, 5]). The potential to additionally texture such films with micro- and nanostructures is highly relevant for biological applications, given that cells are known to sense and respond to the local topology on these length scales [11, 12, 13]. However, these applications are inherently limited to magnetically-induced deformations of several percent. Specifically, strains of up

to 3 % have been measured for Fe-Pd [3, 8], while theoretical values calculated from the lattice constant predict strains near 5 % for single crystals [2].

To achieve strains of over 100 %, smart polymers provide a viable alternative [14]. For example, such materials can be synthesized from the incorporation of magnetic particles to create a magnetically-responsive composite. From the synthesis of highly regular structures on top of a template, there is the possibility to lift-off and chemically detach these structures from the underlying substrate by targeting the interfacial layer [15] or the substrate [9]. Resulting nano- and microparticles exhibiting a magnetic shape anisotropy have potential for bioapplications. Such particles can be used to investigate particle-cell interactions in the presence of applied magnetic fields for purposes such as diagnostics, treatment and sensing devices [16, 17], as well as for the potential to undergo magnetic alignment and embedding in soft polymer matrices to create magnetically deformable materials [18, 19, 20]. The Fe_7Pd_3 alloy is a promising candidate for such applications due to the large magnetocrystalline anisotropy exhibited by two metastable martensitic phases, fct and body centred tetragonal (bct).

For bioapplications, the capacity for cell adhesion and proliferation on a material constitutes the first step to applying these concepts. Fe-Pd thin films have been shown to initiate bioactivity at the surface, particularly through the formation of apatite in physiological conditions [21]. Previously, these films demonstrated excellent proliferation, morphology and adhesion for fibroblasts, epithelial cells and primary osteoblasts cultured directly onto the substrate surface [22]. Furthermore, the impact of irregular surface roughness on cell adhesion and growth was investigated for these surfaces, demonstrating a significant influence over the resulting cell proliferation [22].

With this background, submicron structures of composition Fe_7Pd_3 were synthesized using glancing angle deposition (GLAD) onto substrates. GLAD is a well-established technique for synthesizing micro- and nanostructures with ranging shapes, dimensions and magnetic properties [23, 24, 25], with potential applications of such structures ranging from optoelectronics to biosensing

[26, 27]. Deposited prestructured materials, such as gold, serve as seeds to dictate the size and spacing of the resulting GLAD structures [28]. However, most studies have focused on elemental film synthesis. Recently, several types of alloyed nanostructures have been fabricated using GLAD [29, 30, 31], with few targeting magnetic properties of such an alloy [32]. Here, the viability of GLAD is novelly explored as a technique to synthesis submicron structured films using a ferromagnetic shape memory alloy. Furthermore, alloyed Fe-Pd targets were conveniently used for sputtering, instead of employing individual elemental targets. In the following work, Fe-Pd GLAD submicron rods were synthesized using gold dewetted prestructures and characterized using scanning electron microscopy (SEM), energy-dispersive X-ray spectroscopy (EDS) and X-ray diffraction (XRD).

The influence of the structured Fe-Pd films on cell growth was investigated using human brain microvascular endothelial cells (HBMEC), which are the major component of the human blood-brain barrier [33, 34, 35]. These sensitive endothelial cells constitute a unique cellular barrier in order protect the brain and sustain brain homeostasis [36, 37]. While these cells are commonly implemented in transwell systems to perform permeability assays, they have previously exhibited high sensitivity towards nanoparticle exposure in two-dimensional cell culture [38, 39, 40, 41]. Therefore, HBMEC were seeded on GLAD structures in order to verify whether the submicron structured surfaces significantly effected cell adhesion, morphology and proliferation in comparison to Fe-Pd thin films. Furthermore, the material response to physiological conditions was explored by analyzing the iron and palladium content released into surrounding cell culture medium after incubation and cell growth by inductively coupled plasma optical emission spectrometry (ICP OES). The resulting structures are highly interesting for magnetically-driven applications of textured thin films, studies on cell-particle interactions, and as components in magnetic-polymer composite materials.

Figure 1: The sputtering chamber setup, with micrographs of the gold prestructures and resulting rodlike structures. Illustrations demonstrate how the shadowing effect leads to rodlike growth due to the presence of shadowed regions caused by substrate prestructures. α is the glancing angle between the flux and substrate normal. Figure adapted from Ref. [42].

2. Materials and methods

2.1. Fe-Pd GLAD synthesis

Fe_7Pd_3 submicron rods were grown by DC magnetron sputtering in a sputtering chamber (AJA Int. ATC 1800, base pressure 10^{-9} mbar or better) at glancing incidence onto prestructured surfaces, employing high purity argon at a pressure of 4×10^{-3} mbar. The substrate-to-target distance was 18 cm. Prestructures were synthesized by a thin gold layer onto 500 µm silicon or silicon nitride wafers (100 mm diameter), as indicated. DC magnetron sputter deposition was performed for 50 s and 100 s to obtain 5 nm and 10 nm gold films, respectively, giving a deposition rate of approximately 6.0 nm/min. The sample holder was rotated during deposition at 80 rpm in order to produce homogeneous films. To finalize the prestructures, films were dewetted in air for 30 min at 500 °C. Resulting gold nanoparticles had approximately 50 nm to 100 nm radii, which amounted to roughly 10 times the initial gold film thickness, as

shown in SEM micrograph in Fig. 1. See Ref. [42] for further details regarding the template synthesis.

Glancing angle deposition was investigated using $Fe_{70}Pd_{30}$ and $Fe_{72}Pd_{28}$ targets (ACI Alloys, Inc., San Jose, California) in order to best achieve the desired composition of $Fe_{70}Pd_{30}$, at an angle of incidence of nearly 85°. Films were produced using initial deposition rates of approximately 3 nm/min at 50 W and sputtering times up to 6 h. Deposition rates were monitored frequently, however increased temperatures and subsequently, deposition rates are common over prolonged deposition times. As a result, the deposition was paused as needed to ensure consistency throughout the long sputtering processes. Resulting films reached thicknesses of up to 1.5 µm. For comparison, Fe-Pd thin films with an in-plane composition gradient were produced by combinatorial sputtering onto silicon nitride wafers. These films were approximately 100 nm thick, with a sputtering power of 200 W for the Fe target and 20 W for the Pd target, resulting in a combined deposition rate of 6.1 nm/min.

Annealed was performed on several samples using an evacuated quartz glass tube inside a furnace with < 0.01 mbar base pressure. The environment was purged with argon three times over 15 min, achieving a slight argon overpressure to minimize oxidation during annealing. Annealing was carried out at 900 °C for 10 min once the temperature was reached. The quartz tube was removed from the furnace and the sample allowed to cool at room temperature in a flushed argon environment for at least 2 h.

2.2. Structural analysis

The sample composition was determined by energy-dispersive X-ray spectroscopy (EDS) using a Quanta 250 (FEI Company) and further verified by X-ray diffraction (XRD, Rigaku SmartLab). For calibration of EDS, a reference sample was produced by arc melting 1.534 g iron and 1.259 g palladium. The resulting iron concentration was 54.92 wt%, corresponding to 69.90 at%. From EDS measurements at different positions on the reference sample, the iron content was measured as (68.4 ± 0.7) at%. As a result, a systematic error of 2.2 %

was assumed and all further measurements for the iron content were multiplied by a factor of 1.022 for correction.

The Quanta 250 and a Zeiss Sigma VP were also used to visualize the samples via scanning electron microscopy (SEM). Images were collected in high vacuum mode with acceleration voltages of 5 kV to 25 kV.

The crystal structure was analyzed by XRD with $\theta - 2\theta$ scanning geometry. CuK_α radiation was emitted from the X-ray source at a wavelength of 0.154 nm. Data was fitted using PDXL 2 software with the Crystallography Open Database [43, 44, 45].

2.3. Cell culture

Human brain microvascular endothelial cells (HBMEC) are an established cell line representing the human blood-brain barrier that have demonstrated a high sensitivity to nanoparticle exposure in two-dimensional culture [38, 39, 40]. This adherent cell line, immortalized by introduction of the SV40 large T antigen [33], was used to investigate differences in cellular morphology, adhesion and proliferation on the surfaces of submicron structured Fe-Pd and unstructured Fe-Pd thin films. For the cell-based tests, the structured Fe-Pd samples were produced by GLAD with the $Fe_{72}Pd_{28}$ target onto gold-prestructured Si_3N_4 wafers.

HBMEC were cultivated at 37 °C and 5 % CO_2 in RPMI 1640 medium supplemented with GlutaMAX^{TM} (Life Technologies USA), 10 % (v/v) fetal calf serum (FCS, Biochrom Seromed Berlin, Germany), 100 U/ml penicillin, and 0.1 mg/ml streptomycin (both Life Technologies, USA) in a humidified atmosphere. Fe-Pd structured wafers were sterilized by treating with 10 % (v/v) ethanol for 10 min before 50 000 cells/cm^2 were seeded on the wafers placed within 24 well plates (Greiner Bio-one, Germany) and cultured for 48 h. For controls, both bare Si wafers and Si_3N_4 wafers equipped with unstructured Fe-Pd thin films were seeded with cells analogously.

2.4. Fluorescence staining and laser scanning microscopy

Upon 48 h cultivation, cells were washed three times with phosphate buffered saline (PBS) and fixed in 10 % (v/v) neutral buffered formalin (Sigma-Aldrich Chemie, Germany) for 15 min. Subsequently, the cell membranes were permeabilized in 0.1 % (v/v) Triton X 100 (Sigma-Aldrich, Germany) for 15 min. Both, cytoskeletal F-actin and nuclei were stained simultaneously with Alexa Fluor® 488 Phalloidin and Hoechst33258 (both Invitrogen, Germany) for 60 min at 37 °C. Fluorescence was imaged using the confocal laser scanning microscope LSM 510 META (Carl Zeiss Microscopy GmbH, Germany) using different magnifications. Acquired images were analyzed regarding the cell number and cellular area using the ImageJ 1.45s software (Wayne Rasband, National Institutes of Health, USA) [46].

2.5. Statistics

Statistical significance of cell growth was tested using Prism 6 (GraphPad Software, La Jolla, USA) by one-way analysis of variance (ANOVA) followed by Dunnett's or Tukey's multiple comparison test comparing the means of different cell numbers and areas. Differences were considered to be statistically significant for $p < 0.05$.

2.6. ICP OES

Inductively coupled plasma optical emission spectrometry (ICP OES; Spectro Ciros Vision) was used to determine the iron and palladium content of the growth medium after cell tests. After collection, 1 mL of medium was diluted to 10 mL to ensure sufficient liquid for the measurement. As a result, the elemental detection sensitivity was reduced from $0.008\,\mathrm{mg\,L^{-1}}$ to $0.08\,\mathrm{mg\,L^{-1}}$ for palladium and $0.002\,\mathrm{mg\,L^{-1}}$ to $0.02\,\mathrm{mg\,L^{-1}}$ for iron.

Figure 2: SEM measurements of Fe-Pd structures produced by glancing angle deposition on prestructured Si substrates. See supplementary Fig. S1 for comparable structures on a Si_3N_4 substrate. From top to bottom, a typical dewetted gold template is shown, followed by top views with increasing sputtering time, a tilted view and resulting cross section, as indicated to the left of the images. Top scale bar applies to the four consecutive images. The incoming particle flux is showing at glancing angle α of nearly 85° for the final image.

3. Results

3.1. Prestructures and resulting submicron structures

To obtain submicron, rod-like structured Fe-Pd, glancing angle deposition onto prestructure templates was employed. This technique allows for the growth of such structures due to the shadowing effect of the prestructured template [47, 28]. The geometry of the resulting structures can be tuned directly by the size of the template. Fig. 2 shows SEM images taken at different stages of synthesis, from the initial prestructure template to the final rod growth.

Figure 3: EDS atomic content color maps taken after partial deposition of the iron palladium rod-like structures on a gold-patterned silicon substrate. According to the alignment shown in this image, the sputtering source was located above the image so that the top of the sample was first exposed to the incident particles during deposition.

Using gold dewetting from the substrate, prestructures of radii of approximately 50 nm to 100 nm were achieved from 5 nm and 10 nm homogeneous gold films [42, 48]. Thinner films corresponded to smaller islands formed on the prestructures and resultantly thinner rod growth. The height of the prestructures was approximately 50 nm, with a distance of nearly 500 nm to the nearest neighboring structure. In Fig. 2, a typical template can be seen in the top image. After sputtering for a short amount of time, the second image illustrates the onset of individual structures caused by the shadowing effect. Following sputtering, the resulting directional growth of rod-like structures can be seen in the bottom cross section image. The rods grew progressively thicker, reaching an end radius near 250 nm. Resulting Fe-Pd structures reached heights up to 1.5 µm. However, the individual rods remained separated from each other despite the close proximity, meaning that the structures were not bonded together and detached from one another when released from the substrate.

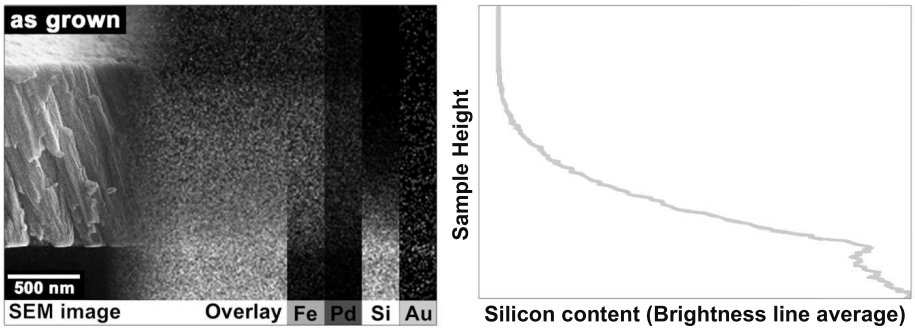

Figure 4: Left, an SEM micrograph of the rodlike structures is shown beside the overlaid and subsequent individual atomic content color maps for each present element, including iron, palladium, silicon and gold. Right, the silicon content (x-axis) is revealed as a progression of the brightness line average as measured by EDS, with the sample height (y-axis) corresponding to the cross section given in the left image.

3.2. Composition

To determine the elemental ratio of the Fe-Pd structures, the resulting compositions from the $Fe_{70}Pd_{30}$ and $Fe_{72}Pd_{28}$ targets were analyzed by EDS with resulting corrected average iron concentrations of $(68.2 \pm 1.0)\,\mathrm{at\%}$ and $(69.4 \pm 1.0)\,\mathrm{at\%}$, respectively. Therefore, the $Fe_{72}Pd_{28}$ target appeared best able to approach the desired $Fe_{70}Pd_{30}$ composition for the structures and was used for further investigations.

Elemental composition maps of the structured samples after partial deposition are shown in Fig. 3. The top side of the sample was positioned nearest to the sputtering source, thus incident particles approached from that direction, as observed by the shape of the resulting columns. Below each structure, shadowed areas are visible with no iron or palladium content. As a result of these shadowed regions, prestructures served as seeds for the growth of individual rods. Inversely, the silicon content was highest in these blocked regions, stemming from the silicon substrate and not from silicon diffusing into the Fe-Pd structures. A weak gold signal was homogeneously observed across the sample surface, which was expected given complete coverage of the gold prestructures. However, given that EDS measurements probe quite deep into the sample, this

gold layer was expected from the substrate coverage and does not necessarily indicate the presence of gold in the rods.

The atomic content of the sample cross section is shown in Fig. 4, as well as the silicon line average obtained from analyzing the brightness of the resulting signal. From this plot, it is clear that the silicon content stemmed from the substrate below the deposited Fe-Pd. The structures were composed mainly of iron and palladium, with trace amounts of gold highest around the interface between the substrate and deposited structures. While a small about of gold appeared throughout the sample height profiles, this signal was likely a measurement artifact of the high acceleration voltage of 25 kV. From quantitative analysis, no significant gold peaks were present in the EDS spectrum throughout the structures. Near the substrate, small amounts of silicon were measured in the lower regions of the Fe-Pd structures. This signal is also likely to be a measurement artifact from EDS instead of a sign of diffused silicon, since the expression varied with acceleration voltages.

XRD measurements were performed to identify the phase of the resulting submicron structures by the X-ray diffraction peaks within the polycrystalline samples deposited from the $Fe_{72}Pd_{28}$ target. $\theta - 2\theta$ scans of the structured samples (further denoted as "rods") and thin film ("film") Fe-Pd samples are plotted in Fig. 5. The samples had a corrected composition of $Fe_{71}Pd_{29}$, which typically corresponds to the bcc phase dominating over fcc. Using lattice constants of 3.75 Å for fcc and 2.93 Å for bcc, the fcc(111), bcc(110), fcc(200), bcc(200), fcc(220) and bcc(211) peaks were determined to occur at $2\theta = 41.7°$, 43.6°, 48.5°, 63.4°, 70.1° and 80.1°, respectively.

Comparing the *as prepared* rods to the continuous thin film, the position of the bcc(110) and bcc(211) peaks shifted to lower angles, indicating larger lattice constants. The bcc(110) peak in the structured sample corresponded to a lattice constant of 2.96 Å ($2\theta = 43.1°$), while its continuous thin film counterpart was determined as 2.93 Å ($2\theta = 43.6°$). Furthermore, the fcc(111) peak was slightly visible in the film, but not in the rods. Other than from the Fe-Pd, no other peaks were observed. Overall, the *as prepared* Fe-Pd polycrystalline samples

Figure 5: XRD $\theta - 2\theta$ measurements for $Fe_{71}Pd_{29}$ *as prepared* (denoted by "0") and 900 °C annealed (denoted by "900") submicron structured rods (R) and continuous thin film (F). The structures were synthesized by GLAD with the $Fe_{72}Pd_{28}$ target onto prestructured Si substrates, while the unstructured thin film was produced by combinatorial sputtering onto Si_3N_4. Data was corrected for background noise and normalized to the largest peak, with the smooth lines representing fits. Peak positions were determined from the Crystallography Open Database[43, 44, 45].

mainly exhibited crystal structures consistent with the bcc phase.

The thin film and structured substrates were annealed at 900 °C. Resulting XRD spectra are also shown in Fig. 5. After annealing, bcc(110) and bcc(211) peaks disappeared for both the thin and submicron structured films. In the case of the structured films, new peaks were observed, namely (111) at $2\theta = 41.4°$, (200) at $2\theta = 48.9°$, (220) at $2\theta = 71.2°$ and (311) at $2\theta = 86.2°$. The most prominent peak in the annealed rod-like sample was the (220), indicating a corresponding texture. The slight shift of the (200) peak from the perfect fcc (200) angle might indicate presence of a single variant fct martensitic phase with the short axis aligned normal to the surface, as discussed previously [9].

However, extended annealing times also resulted in diffusive sintering of the structures, as shown in Fig. S2 and S3.

The annealed thin film expressed two peaks at $2\theta = 47.7°$ and $2\theta = 48.9°$ around the fcc(200) position, which are consistent with multivariate fct martensite, plus some additional peaks identified as Fe_2SiO_4 (020), (022), (013) and (210), resulting from sputter deposition onto the Si_3N_4 substrate. These signals were notably absent in the rod spectra, given the thin film samples were considerably thinner than the rod-like structures.

In summary, the samples initially exhibited peaks primarily corresponding to the bcc phase, which shifted upon annealing to indicate the presence of fcc / fct phase in both the thin film and submicron structured rods. Potential measures to maintain structural integrity during annealing include lift-off of the structures prior to annealing or application of laser assisted ultra-rapid treatment.

3.3. Cellular responses

In order to investigate the influence of the submicron structured Fe-Pd on cell adhesion, morphology and proliferation, HBMEC were used as a typical representation of the blood-brain barrier. Cells were seeded on Fe-Pd-sputtered Si_3N_4 wafers, cultivated for 48 h, fluorescently stained and then analyzed microscopically. The microscopic images shown in Fig. 6 reveal that these sensitive cells adhered to all surfaces uniformly regardless of whether the substrates were uncoated, equipped with a thin Fe-Pd film or sputtered with Fe-Pd rod-like structures. Furthermore, cells proliferated similarly as the average numbers of cells found on all surfaces did not differ significantly upon cultivation for 48 h. More detailed cell analysis indicates a well-distributed cell morphology with large cell nuclei and pronounced cell-cell contacts for bare surfaces as well as structured Fe-Pd surfaces. The average cell area was not affected by cellular growth on Fe-Pd rod-like structures, as indicated by the lower panel of Fig. 6. It should be noted that the average cell number cultured on both Fe-Pd samples and Si controls 48 h after cell seeding was reduced by 40 % to 50 % compared to cells seeded on conventional glass cover slips (data shown in supplementary

Figure 6: HBMEC were seeded on Si wafers without Fe-Pd coating (Si, second column), Si_3N_4 wafers with unstructured Fe-Pd thin films (Si_3N_4 & Fe-Pd film, third column), or submicron structured Fe-Pd on Si_3N_4 wafers (Si_3N_4 & Fe-Pd str., fourth column). Upon fixation and permeabilization, nuclei and F-actin were stained with Hoechst33258 (blue) and Alexa Fluor-Phalloidin® 488 (green), respectively. For background controls, cell-free structured Fe-Pd Si_3N_4 wafers were stained analogously (w/o HBMEC, first column). All samples were analyzed by confocal laser scanning microscopy with 100-fold and 400-fold magnification where scale bars indicate 100 µm and 20 µm, respectively. 400-fold magnified images were analyzed regarding cell numbers and cell areas. Results show the mean ± standard deviation of three different fields of view.

Sample	Iron ($\mathrm{mg\,L^{-1}}$)	Palladium ($\mathrm{mg\,L^{-1}}$)
Medium (no cells)	0.023 ± 0.001	$<0.002 \pm 0.003$
Glass control	0.159 ± 0.011	$<0.030 \pm 0.026$
Fe-Pd GLAD (no cells)	0.199 ± 0.008	$<0.027 \pm 0.024$
Fe-Pd GLAD	0.203 ± 0.008	$<0.061 \pm 0.026$
Fe-Pd thin film	0.209 ± 0.006	$<0.021 \pm 0.020$

Table 1: Measured iron and palladium contents for cell culture medium, as determined by ICP OES, after cell tests were preformed with the given samples. Uncertainties represent one standard deviation of 3 to 9 measurements, while <indicates the measured values were below the detection threshold.

Fig. S4 and S5).

Using ICP OES, the iron and palladium content in the surrounding cell culture medium was analyzed following the period of cell growth. In table 1, the measured amounts are given for the following controls: culture medium and Fe-Pd GLAD structures, both incubated without cells, and cell growth on a glass control and Fe-Pd thin film.

Iron content in the medium significantly increased from $(0.023 \pm 0.001)\,\mathrm{mg\,L^{-1}}$ to $(0.159 \pm 0.011)\,\mathrm{mg\,L^{-1}}$ between the controls without and with cells. There was a minor increase in the iron content between the control medium (glass substrate with cells) and the Fe-Pd samples (GLAD structures and thin film, both on Si_3N_4), from $(0.159 \pm 0.011)\,\mathrm{mg\,L^{-1}}$ to near $0.2\,\mathrm{mg\,L^{-1}}$, respectively. This difference is equivalent to an increase of 25 % to 32 % in the iron content for the respective Fe-Pd GLAD structures and thin film, compared to the control. A detected iron increase of approximately $0.04\,\mathrm{mg\,L^{-1}}$ is less than 0.01 % of the sample iron content, assuming a sample height of 1 µm. However, there were no significant differences in the iron content of the medium from the Fe-Pd GLAD structures (with and without cells) or Fe-Pd thin film.

The palladium content measured for all the samples was below the instrument detection limit. The pure culture medium without cells had the lowest palladium content of $(0.002 \pm 0.003)\,\mathrm{mg\,L^{-1}}$, which was an order of magnitude

smaller than measured for all other samples. That in mind, there were no significant differences in the palladium content for any of the samples when considering the deviation in consecutive measurements. This uncertainty was on the order of the measured value, given the close proximity to the device detection threshold. These results are in good agreement with the previous work of [21], where negligible palladium and comparably small amounts of iron were released from Fe-Pd thin films in simulated body fluid over a 65 h period.

4. Discussion

GLAD was used to synthesize rod-like submicron structured Fe-Pd on top of prestructured gold films. Using these templates, the shadowing effect led to the growth of rod-like features of several hundred nanometers width and lengths up to 1.5 µm. Varying the template resulted in different widths for the Fe-Pd rod-like structures. Further modifications to the prestructured template or other techniques such as motion of the substrate during growth could potentially achieve other architectures for the structured film [42, 23, 24]. While rod-like structures were achieved on gold-prestructured Si and Si_3N_4, the role of the substrate material in resulting architectures should be investigated further in order to potentially realize enhanced geometries. The rod length was limited by the sputtering time and target material. This length could be increased if the sputtering process was continued to achieve longer structures with a higher shape anisotropy.

The $Fe_{72}Pd_{28}$ target resulted in structures approaching 70 at% iron, as quantified by EDS. Silicon from the substrate and gold from the prestructures were largely constrained to the interfacial region, with only trace amounts detected in the lower region of the Fe-Pd structures. For further verification, XRD measurements were taken to analyze the material composition and crystal structure of the submicron structured and thin film Fe-Pd. The composition was corrected to $Fe_{71}Pd_{29}$ and exhibited peaks corresponding to the bcc phase.

In order to realize magnetically-induced reorientation of twin variants in

Fe-Pd, the alloy must be composed of approximately 30 at% palladium so that material crystallization under rapid cooling results in fct martensite. While the Fe-Pd composition of the submicron structures approached $Fe_{70}Pd_{30}$, the material did not exhibit the necessary fct phase when deposited at room temperature. However, upon subsequent annealing at 900 °C [49, 50], the samples appeared to undergo the desired transformation, as visible in Fig. 5.

This transition to the fct phase was indicated by the consistent position of the fcc(111) peak before and after annealing, combined with splitting and/or shifting of the fcc(200) and fcc(220) peaks into respective fct(200)/(020) and fct(002), as well as fct(220) and fct(022)/(202). Both the film and rod-like structures exhibited shifts in these peaks that allowed for recalculation of the lattice constants with respect to the a and c axes. The resulting a/c ratio for the annealed samples was 0.988, indicating that a weak tetragonal distortion was present [2]. The martensite transition temperature is sensitive to the annealing conditions as well as substrate presence, as shown in [10, 51] for respective single crystalline Fe-Pd films and polycrystalline Fe-Pd foils. Studies of the shape memory and magnetic shape memory effects, including the thermally induced phase transition, will be the focus of future studies. While a multiple variant fct phase was obtained in the films after annealing at 900 °C, the structures underwent - at least partially - a phase transition to single variant fct during quenching and the well-defined structures were destroyed (see Fig. S2 and S3). Therefore, in order to obtain the desired fct phase while preserving structural features, ultrarapid heating or laser heating should be utilized [52]. Alternatively, structures could be detached and dispersed in an appropriate medium before annealing to prevent breakdown.

Cell tests with highly sensitive HBMEC did not reveal reduced adhesion or proliferation after 48 h on the structured Fe-Pd samples, compared to Fe-Pd thin films or the control Si substrate. However, both types of Fe-Pd samples and the Si control exhibited an inhibitory effect or delayed initiation of proliferation in comparison to culturing on glass. A reduced proliferation of fibroblasts on Fe-Pd was previously observed in [22], without any signs of cytotoxicity,

and was attributed to additional time required for adaptation and adhesion to the substrates. Cell cycle analysis and cell viability assays would provide further insight into the general reduction in proliferation on Fe-Pd as a next step. Overall, the HMBEC response to the Fe-Pd samples demonstrated healthy cell morphologies, large nuclei and well-balanced intercellular contacts, regardless of the structuring and sputtering approach.

In support of this conclusion, the surrounding medium did not show cytotoxic elemental levels of iron or palladium following the cell tests. The palladium content released from the samples over this period was negligible, while the iron content increased by up to 32 % compared to the controls. However, the submicron structured films did not have significantly higher iron content released compared to the Fe-Pd thin film, despite having increased surface area due to the individual structures. While the corrosion of pure iron can result in the formation of harmful radicals [53, 54], *in vivo* experiments using rabbits demonstrated safe implantation of pure iron stents [55]. In that case, the material corroded at a much higher rate of nearly $20\,\mu g\,cm^{-2}\,h^{-1}$ for human endothelial cells. Potential cytotoxicity was not observed until over $50\,mg\,L^{-1}$, which is orders of magnitude above the amounts detected from the Fe-Pd samples. In contrast, the Fe-Pd samples in the above experiments released less than $1\,ng\,cm^{-2}\,h^{-1}$, with enhanced stability as a direct result of alloying with the noble metal palladium. Furthermore, this iron content is well within the acceptable limits as defined by the Food and Nutrition Board of the USA, which gives an upper tolerant intake level of $45\,mg\,d^{-1}$ for adult human consumption based on the onset of gastrointestinal distress [56].

Future work will focus on the unique magnetic properties of such structures, while working to achieve a wider range of shapes and dimensionality through GLAD synthesis investigating various prestructured templates. Annealing strategies to undergo the desired phase transformation while maintaining the defined structures should be refined. Additionally, lift-off of the structures should be attempted, opening up a wide range of interesting applications for shape-anisotropic magnetic micro- and nanoparticles.

5. Conclusions

GLAD is a promising method to control the synthesis of structured Fe-Pd films. This study demonstrates the viability of applying this synthesis method to alloyed materials. Given the sensitivity of the Fe-Pd system as a result of a very shallow energy barrier between phases, this methodology should be applicable to a range of other alloys. Resulting rod-like submicron structures were predominantly in the bcc phase, with a composition approaching $Fe_{70}Pd_{30}$. Annealing at 900 °C achieved the fct phase, but required further tuning using methods such as ultrarapid heating, laser irradiation or lift-off prior to annealing to preserve the desired structures. Consistent cell adhesion, proliferation and morphologies of HBMEC were demonstrated on various Fe-Pd surfaces, independent of structuring. Very limited release of iron and negligible palladium over the 48 h period reinforced these results. Overall, this method exhibits high promise for the development of biocompatible, shape-anisotropic magnetic structures or textured films composed of Fe-Pd.

6. Acknowledgements

SEM and XRD measurements by Ellen Scanley (Southern Connecticut State University) and Jingbei Liu (Yale School of Engineering and Applied Science) are gratefully acknowledged. This project was funded in parts by the German Science Foundation (DFG) - SPP 1681 (MA 2432/6 and CL 202/3), the German Academic Exchange Service (DAAD) and the Natural Sciences and Engineering Research Council of Canada (NSERC) through a PGS D. Film fabrication and structural characterization was funded by NSF-DMREF #DMR-1436268.

References

[1] F. Ono, T. Kittaka, H. Maeta, Thermal expansion measurements in Fe-base invar alloys, Physica B+C 119 (1) (1983) 78–83.

[2] J. Cui, T. W. Shield, R. D. James, Phase transformation and magnetic anisotropy of an iron–palladium ferromagnetic shape-memory alloy, Acta Materialia 52 (1) (2004) 35–47.

[3] R. D. James, M. Wuttig, Magnetostriction of martensite, Philosophical Magazine A 77 (5) (1998) 1273–1299.

[4] T. R. Vogel, L. E. Shindelman, G. B. Nackman, A. M. Graham, Efficacious use of nitinol stents in the femoral and popliteal arteries, Journal of Vascular Surgery 38 (6) (2003) 1178–1183.

[5] M. Zink, S. G. Mayr, Ferromagnetic shape memory alloys: synthesis, characterisation and biocompatibility of Fe–Pd for mechanical coupling to cells, Materials Science and Technology 30 (13) (2014) 1579–1589.

[6] R. Rushforth, Palladium in Restorative Dentistry, Platinum Metals Review 48 (1) (2004) 30–31.

[7] D. P. Whittle, J. Stringer, Improvements in High Temperature Oxidation Resistance by Additions of Reactive Elements or Oxide Dispersions, Philosophical Transactions of the Royal Society of London A: Mathematical, Physical and Engineering Sciences 295 (1413) (1980) 309–329.

[8] J. Koeda, Y. Nakamura, T. Fukuda, T. Kakeshita, T. Takeuchi, K. Kishio, Giant magnetostriction in Fe-Pd alloy single crystal exhibiting martensitic transformation, Transactions-Materials Research Society of Japan 26 (1) (2001) 215–218.

[9] T. Edler, S. G. Mayr, Film Lift–Off from MgO: Freestanding Single Crystalline Fe–Pd Films Suitable for Magnetic Shape Memory Actuation – and Beyond, Advanced Materials 22 (44) (2010) 4969–4972.

[10] Y. Ma, A. Setzer, J. W. Gerlach, F. Frost, P. Esquinazi, S. G. Mayr, Freestanding Single Crystalline Fe–Pd Ferromagnetic Shape Memory Membranes – Role of Mechanical and Magnetic Constraints Across the Martensite Transition, Advanced Functional Materials 22 (12) (2012) 2529–2534.

[11] A. Curtis, C. Wilkinson, Topographical control of cells, Biomaterials 18 (24) (1997) 1573–1583.

[12] R. G. Flemming, C. J. Murphy, G. A. Abrams, S. L. Goodman, P. F. Nealey, Effects of synthetic micro- and nano-structured surfaces on cell behavior, Biomaterials 20 (6) (1999) 573–588.

[13] M. Nikkhah, F. Edalat, S. Manoucheri, A. Khademhosseini, Engineering microscale topographies to control the cell-substrate interface, Biomaterials 33 (21) (2012) 5230–5246.

[14] W. Voit, T. Ware, R. R. Dasari, P. Smith, L. Danz, D. Simon, S. Barlow, S. R. Marder, K. Gall, High-Strain Shape-Memory Polymers, Advanced Functional Materials 20 (1) (2010) 162–171.

[15] C. Bechtold, J. Buschbeck, A. Lotnyk, B. Erkartal, S. Hamann, C. Zamponi, L. Schultz, A. Ludwig, L. Kienle, S. Fähler, E. Quandt, Artificial Single Variant Martensite in Freestanding $Fe_{70}Pd_{30}$ Films Obtained by Coherent Epitaxial Growth, Advanced Materials 22 (24) (2010) 2668–2671.

[16] T. D. Schladt, K. Schneider, H. Schild, W. Tremel, Synthesis and bio-functionalization of magnetic nanoparticles for medical diagnosis and treatment, Dalton Transactions 40 (24) (2011) 6315–6343.

[17] S. Nath, C. Kaittanis, V. Ramachandran, N. S. Dalal, J. M. Perez, Synthesis, Magnetic Characterization, and Sensing Applications of Novel Dextran-Coated Iron Oxide Nanorods, Chemistry of Materials 21 (8) (2009) 1761–1767.

[18] S. Monz, A. Tschöpe, R. Birringer, Magnetic properties of isotropic and anisotropic $CoFe_2O_4$-based ferrogels and their application as torsional and rotational actuators, Physical Review E 78 (2) (2008) 021404.

[19] P. Bender, A. Tschöpe, R. Birringer, Magnetization measurements reveal the local shear stiffness of hydrogels probed by ferromagnetic nanorods, Journal of Magnetism and Magnetic Materials 372 (2014) 187–194.

[20] T. Kimura, Y. Umehara, F. Kimura, Magnetic field responsive silicone elastomer loaded with short steel wires having orientation distribution, Soft Matter 8 (23) (2012) 6206–6209.

[21] Y. Ma, M. Zink, S. G. Mayr, Biocompatibility of single crystalline $Fe_{70}Pd_{30}$ ferromagnetic shape memory films, Applied Physics Letters 96 (21) (2010) 213703.

[22] U. Allenstein, Y. Ma, A. Arabi-Hashemi, M. Zink, S. G. Mayr, Fe-Pd based ferromagnetic shape memory actuators for medical applications: Biocompatibility, effect of surface roughness and protein coatings, Acta Biomaterialia 9 (3) (2013) 5845–5853.

[23] K. Robbie, M. Brett, Sculptured thin films and glancing angle deposition: Growth mechanics and applications, Journal of Vacuum Science & Technology A 15 (3) (1997) 1460–1465.

[24] K. Robbie, J. C. Sit, M. J. Brett, Advanced techniques for glancing angle deposition, Journal of Vacuum Science & Technology B 16 (3) (1998) 1115–1122.

[25] O. Albrecht, R. Zierold, S. Allende, J. Escrig, C. Patzig, B. Rauschenbach, K. Nielsch, D. Görlitz, Experimental evidence for an angular dependent transition of magnetization reversal modes in magnetic nanotubes, Journal of Applied Physics 109 (9) (2011) 093910.

[26] A. Yildiz, H. Cansizoglu, M. Turkoz, R. Abdulrahman, A. Al-Hilo, M. F. Cansizoglu, T. M. Demirkan, T. Karabacak, Glancing angle deposited Al-doped ZnO nanostructures with different structural and optical properties, Thin Solid Films 589 (2015) 764–769.

[27] S. K. Srivastava, H. B. Hamo, A. Kushmaro, R. S. Marks, C. Grüner, B. Rauschenbach, I. Abdulhalim, Highly sensitive and specific detection of E. coli by a SERS nanobiosensor chip utilizing metallic nanosculptured thin films, The Analyst 140 (9) (2015) 3201–3209.

[28] J. Bauer, M. Weise, B. Rauschenbach, N. Geyer, B. Fuhrmann, Shape evolution in glancing angle deposition of arranged Germanium nanocolumns, Journal of Applied Physics 111 (10) (2012) 104309.

[29] S. Chen, Z. Li, Z. Zhang, Anisotropic $Ti_xSn_{1-x}O_2$ nanostructures prepared by magnetron sputter deposition, Nanoscale Research Letters 6 (1) (2011) 326.

[30] S. Chen, Z. Li, Z. Zhang, The novel wetting behavior of periodic $Ti_xSn_{1-x}O_2$ nanostructures, Materials Transactions 53 (1) (2012) 191–194.

[31] N. N. Kariuki, W. J. Khudhayer, T. Karabacak, D. J. Myers, GLAD Pt–Ni Alloy Nanorods for Oxygen Reduction Reaction, ACS Catalysis 3 (12) (2013) 3123–3132.

[32] S. Kitai, Z. Zheng-Jun, S. Ji, Y. Nakamura, Characterization of CoPt nanowire fabricated by glancing angle deposition, Chinese Physics B 24 (5) (2015) 56201.

[33] M. F. Stins, J. Badger, K. Sik Kim, Bacterial invasion and transcytosis in transfected human brain microvascular endothelial cells, Microbial Pathogenesis 30 (1) (2001) 19–28.

[34] D. E. Eigenmann, G. Xue, K. S. Kim, A. V. Moses, M. Hamburger, M. Oufir, Comparative study of four immortalized human brain capillary endothelial cell lines, hCMEC/D3, hBMEC, TY10, and BB19, and optimization of culture conditions, for an in vitro blood-brain barrier model for drug permeability studies, Fluids and barriers of the CNS 10 (1) (2013) 33.

[35] J. Bicker, G. Alves, A. Fortuna, A. Falcão, Blood–brain barrier models and their relevance for a successful development of CNS drug delivery systems: A review, European Journal of Pharmaceutics and Biopharmaceutics 87 (3) (2014) 409–432.

[36] T. S. Reese, M. J. Karnovsky, Fine structural localization of a blood-brain barrier to exogenous peroxidase, The Journal of Cell Biology 34 (1) (1967) 207–217.

[37] C. Crone, S. P. Olesen, Electrical resistance of brain microvascular endothelium, Brain Research 241 (1) (1982) 49–55.

[38] C. Gräfe, I. Slabu, F. Wiekhorst, C. Bergemann, F. v. Eggeling, A. Hochhaus, L. Trahms, J. H. Clement, Magnetic particle spectroscopy allows precise quantification of nanoparticles after passage through human brain microvascular endothelial cells, Physics in Medicine and Biology 61 (11) (2016) 3986.

[39] F. Bähring, F. Schlenk, J. Wotschadlo, N. Buske, T. Liebert, C. Bergemann, T. Heinze, A. Hochhaus, D. Fischer, J. H. Clement, Suitability of Viability Assays for Testing Biological Effects of Coated Superparamagnetic Nanoparticles, IEEE Transactions on Magnetics 49 (1) (2013) 383–388.

[40] A. Theumer, C. Gräfe, F. Bähring, C. Bergemann, A. Hochhaus, J. H. Clement, Superparamagnetic iron oxide nanoparticles exert different cytotoxic effects on cells grown in monolayer cell culture versus as multicellular spheroids, Journal of Magnetism and Magnetic Materials 380 (2015) 27–33.

[41] M. Zhou, T. Liebert, R. Müller, A. Dellith, C. Gräfe, J. H. Clement, T. Heinze, Magnetic Biocomposites for Remote Melting, Biomacromolecules 16 (8) (2015) 2308–2315.

[42] Y. Liu, J. Liu, S. Sohn, Y. Li, J. J. Cha, J. Schroers, Metallic glass nanostructures of tunable shape and composition, Nature Communications 6 (2015) 7043.

[43] S. Gražulis, A. Daškevič, A. Merkys, D. Chateigner, L. Lutterotti, M. Quirós, N. R. Serebryanaya, P. Moeck, R. T. Downs, A. Le Bail, Crystallography Open Database (COD): an open-access collection of crystal

structures and platform for world-wide collaboration, Nucleic Acids Research 40 (D1) (2012) D420–D427.

[44] S. Gražulis, D. Chateigner, R. T. Downs, A. F. T. Yokochi, M. Quirós, L. Lutterotti, E. Manakova, J. Butkus, P. Moeck, A. Le Bail, Crystallography Open Database – an open-access collection of crystal structures, Journal of Applied Crystallography 42 (4) (2009) 726–729.

[45] R. T. Downs, M. Hall-Wallace, The American Mineralogist Crystal Structure Database, American Mineralogist 88 (2003) 247–250.

[46] C. A. Schneider, W. S. Rasband, K. W. Eliceiri, NIH Image to ImageJ: 25 years of image analysis, Nature Methods 9 (7) (2012) 671–675.

[47] M. M. Hawkeye, M. J. Brett, Glancing angle deposition: Fabrication, properties, and applications of micro- and nanostructured thin films, Journal of Vacuum Science & Technology A 25 (5) (2007) 1317–1335.

[48] D. Kim, A. L. Giermann, C. V. Thompson, Solid-state dewetting of patterned thin films, Applied Physics Letters 95 (25) (2009) 251903.

[49] H. Nakajima, T. Okazaki, T. Kubota, M. Sato, Y. Furuya, Phase Transformation in Rapidly Solidified Fe-29.6 at%Pd Ribbons, Materials Transactions 45 (8) (2004) 2752–2756.

[50] J. Buschbeck, S. Hamann, A. Ludwig, B. Holzapfel, L. Schultz, S. Fähler, Correlation of phase transformations and magnetic properties in annealed epitaxial Fe–Pd magnetic shape memory alloy films, Journal of Applied Physics 107 (11) (2010) 113919.

[51] I. Kock, S. Hamann, H. Brunken, T. Edler, S. Mayr, A. Ludwig, Development and characterization of $Fe_{70}Pd_{30}$ ferromagnetic shape memory splats, Intermetallics 18 (5) (2010) 877–882.

[52] A. Arabi-Hashemi, M. Ehrhardt, P. Lorenz, D. Hirsch, K. Zimmer, S. G. Mayr, Epitaxy from the liquid phase: tuning metastable phases in Fe–Pd

thin films by laser-assisted rapid solidification on substrates, Journal of Physics D: Applied Physics 47 (41) (2014) 415302.

[53] S. Zhu, N. Huang, L. Xu, Y. Zhang, H. Liu, H. Sun, Y. Leng, Biocompatibility of pure iron: In vitro assessment of degradation kinetics and cytotoxicity on endothelial cells, Materials Science and Engineering: C 29 (5) (2009) 1589–1592.

[54] A. W. Girotti, Lipid hydroperoxide generation, turnover, and effector action in biological systems, Journal of Lipid Research 39 (8) (1998) 1529–1542.

[55] M. Peuster, P. Wohlsein, M. Brügmann, M. Ehlerding, K. Seidler, C. Fink, H. Brauer, A. Fischer, G. Hausdorf, A novel approach to temporary stenting: degradable cardiovascular stents produced from corrodible metal—results 6–18 months after implantation into New Zealand white rabbits, Heart 86 (5) (2001) 563–569.

[56] Food and Nutrition Board, Institute of Medicine, Dietary Reference Intakes for Vitamin A, Vitamin K, Arsenic, Boron, Chromium, Copper, Iodine, Iron, Manganese, Molybdenum, Nickel, Silicon, Vanadium, and Zinc, National Academies Press, Washington, D.C., 2001.
URL http://www.nap.edu/catalog/10026

Binary Fe-Pd submicron structures fabricated through glancing angle deposition (GLAD) for bioapplications
Supplementary Information

Uta Allenstein[a,b,1], Emilia I. Wisotzki[a,1], Christine Gräfe[c], Joachim H. Clement[c], Yanhui Liu[b], Jan Schroers[b], S. G. Mayr[a,*]

[a] *Leibniz-Institute for Surface Modification (IOM), Leipzig, Germany and Division of Surface Physics, Department of Physics and Earth Sciences, University of Leipzig, Germany*
[b] *Department of Mechanical Engineering and Materials Science, Yale University, New Haven, Connecticut 06511, USA*
[c] *Clinic of Internal Medicine II, Department of Haematology and Medical Oncology, Jena Universital Hospital, Jena, Germany*

[*] Corresponding author
[1] Shared first authorship

Structured Fe-Pd on Si_3N_4 wafers

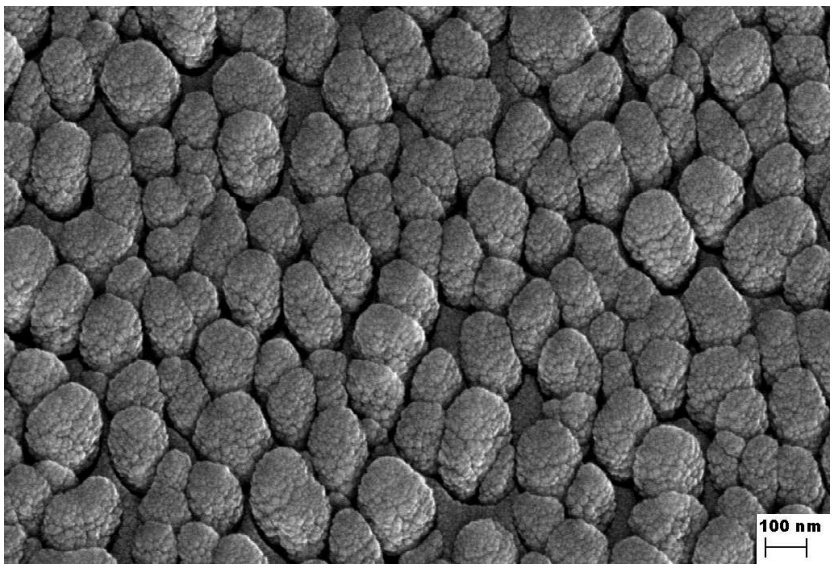

Figure S1: Top view of the structured Fe-Pd by GLAD onto gold-prestructured Si_3N_4 wafers, from an $Fe_{72}Pd_{28}$ target.

Annealing of the structured Fe-Pd

Figure S2: Cross section and top views of the submicron structured Fe-Pd before and after annealing at 900 °C. Although multiple variant fct phase was obtained in the films after annealing at this temperature, the structures underwent a phase transition during quenching, resulting in loss of the well-defined structures. To obtain the fct phase and preserve structural features, ultrarapid heating or laser heating should be employed.

Figure S3: Top SEM and EDS views of the 900 °C annealed Fe-Pd structures, showing a loss of the submicron structures previously observed by the Fe, Pd and Si content (Fig. 3).

Cellular results in comparison to glass control

Figure S4: HBMEC seeded onto glass controls, shown here in comparison to cells grown on structured Fe-Pd on Si_3N_4 wafers. The cell area could not be analyzed due to the high degree of surface coverage on the glass samples. Upon fixation and permeabilization, nuclei and F-actin were stained with Hoechst33258 (blue) and Alexa Fluor-Phalloidin® 488 (green), respectively. All samples were analyzed by confocal laser scanning microscopy with 100-fold and 400-fold magnification where scale bars indicate 100 µm and 20 µm, respectively.

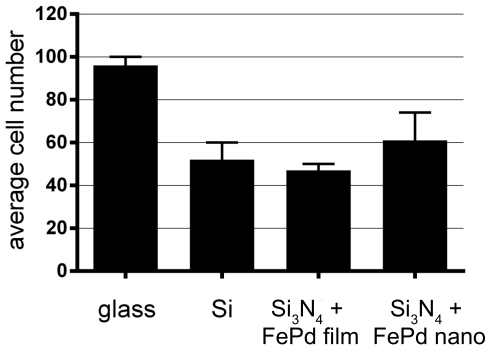

Figure S5: From analysis of the 400-fold magnified images, the average cell counts were determined for the various samples. The total cell counts on Si and Fe-Pd samples were reduced by approximately 40 % to 50 % in comparison to on the glass control. These reductions in the cell counts obtained from the glass control and all other films were statistically significant.